

Study of the dielectric function of PbSnTe epitaxial film by far-infrared reflectivity*

W. E. Tennant and J. A. Cape

Rockwell International, Science Center, Thousand Oaks, California 91360

(Received 15 September 1975)

Far-infrared reflectivity measurements have been carried out from ~ 40 to 320 cm^{-1} on a $\text{Pb}_{0.88}\text{Sn}_{0.12}\text{Te}$ epitaxial film of low carrier concentration ($p \sim 10^{16}\text{ cm}^{-3}$) on a high-carrier-density ($p \sim 10^{18}\text{ cm}^{-3}$) $\text{Pb}_{0.78}\text{Sn}_{0.22}\text{Te}$ substrate. The reflectivity data were analyzed using a two-oscillator dielectric function including free-carrier and phonon linewidths. An upper bound for the LO-phonon frequency was determined to be 115.7 cm^{-1} at room temperature and 113.5 cm^{-1} at liquid- N_2 temperature. Other parameters obtained were the phonon linewidth $\gamma = 19\text{ cm}^{-1}$ at room temperature and 12 cm^{-1} at liquid- N_2 temperature, and the substrate free-carrier linewidth $\nu = 81\text{ cm}^{-1}$ at room temperature and $\sim 70\text{ cm}^{-1}$ at liquid- N_2 temperature. An analysis of the oscillatory behavior of the reflectivity at frequencies above the highest plasmon-phonon mode permitted the determination of the spatial variation of carrier concentration in the region of the film-substrate interface.

INTRODUCTION

The strong interaction of phonons, free carriers, and bound charges in PbSnTe alloys has caused them to be widely studied from the standpoint of fundamental solid-state physics. Moreover the performance of PbSnTe devices near zero frequency depends critically on the dielectric properties determined by these interacting phenomena. The lattice modes of the system are of particular interest because the materials are paraelectric and for sufficiently large Sn concentrations they become ferroelectric.

In a polar semiconductor the optical-mode frequencies are modified by interaction with the free carriers.^{1,2} The effect is greatest for the zone-center ($q=0$) optical modes which determine the far-infrared reflectivity. Bulk crystals of PbSnTe generally grow with sufficiently large carrier densities that the $q=0$ dielectric function is dominated by the free-carrier plasma. Unless the carrier density is $\lesssim 10^{16}\text{ cm}^{-3}$ the longitudinal mode is strongly screened and cannot be determined by conventional far-infrared techniques. Carrier densities of this level and lower have been achieved in liquid-phase epitaxial films.³⁻⁵

In such low-carrier-density materials, the reflectivity approximates nearly the ideal "restrahl" behavior, rising sharply at frequencies below the unscreened longitudinal optical mode ω_L . Preliminary results of some of our measurements on such epitaxial films have been reported previously.⁶

Thin transparent films on a transparent or reflecting substrate of a few wavelengths' thickness show oscillations in reflectivity characteristic of interference between radiation reflected from the two film surfaces. Therefore in addition to determining some of the phonon parameters, the analysis of reflectivity of the film-substrate system in the frequency range above ω_L yields in-

formation about the spatial variation of the carrier concentration in the interface region. The analytical methods used herein should be applicable to many semiconductor heterojunctions and homojunctions where a nondestructive determination of the carrier concentration profile is required.

The present work presents a more complete analysis of the film studied earlier⁶ and corrects some errors in the earlier work.

EXPERIMENTAL

The $\text{Pb}_{1-x}\text{Sn}_x\text{Te}$ sample was a p -type epitaxial layer grown by liquid-phase epitaxy on a p^+ substrate. X-ray determination of the lattice spacing gave values of x equal to 12% ($\pm 2\%$) for the film and 22% ($\pm 2\%$) for the substrate.⁷

The reflectivity measurements were made using a Beckman FS 720 Fourier-transform spectrophotometer which had been modified to accommodate reflectivity samples at liquid-nitrogen temperatures as well as at room temperature. Data were taken and partially processed in real time by a dedicated PDP 11/05 NC digital computer with 16×10^3 -word memory, a 1.2-megaword disk unit, and high-speed paper tape storage and input-output capabilities. A monitor scope was attached to the system for real-time monitoring and display convenience. The system provided on-line data acquisition, Fourier-transformation, phase correction, ratioing, and averaging capabilities. Data reduction and analysis were done with the same computer.

Spectra of the film were taken with resolution of $\approx 10\text{ cm}^{-1}$, a value sufficient to resolve all spectral features. For substrate spectra 20 cm^{-1} was sufficient to see the minimum in reflectivity associated with the plasma frequency. The small sample size ($\lesssim 2\text{-mm-diam}$ usable area) caused light below 40 cm^{-1} to be diffracted out of the beam, prohibiting accurate measurements below

this frequency. The accessible spectral range of our apparatus was limited at high frequencies by the 350 cm^{-1} cutoff of the cooled black polyethylene and sapphire window in front of the doped silicon bolometer.

Normally, three or four spectra were taken at room temperature and at liquid-nitrogen temperature without moving the sample. Reference spectra of an aged, front-surface aluminum mirror (nominal reflectivity 0.985 in this region⁸) were taken close in time to the sample spectrum to reduce any effects of bolometer drift which might have been present. In fact, no bolometer drift appeared on a scale of several hours. Noise on the spectra was averaged to yield a standard deviation for the spectral points.

Ratios of sample spectra (S_{ni}) to reference mirror (S_{di}) spectra were obtained and standard deviations in the ratio of data points ($r_i = S_{ni}/S_{di}$) were computed according to the formula

$$\Delta r_i = [(\Delta S_{ni}/S_{di})^2 + (\Delta S_{di} S_{ni}/S_{di}^2)^2]^{1/2}. \quad (1)$$

Errors in mirror positioning, surface irregularities, small shifts in the sample position upon cooling, and lack of a calibrated reference mirror combined to make the normalization of the reflected spectrum uncertain to a few percent.

To circumvent these difficulties, the final normalization factor was established by requiring a best fit to the experimental data in and near the restrahl region where the reflectivity is greatest and least complicated by effects of roughness and interference (see discussion below). The computed normalization factor was 0.976 for the low-temperature data and 0.99 for the room-temperature data. Taking into account the nominal mirror reflectivity, this implies that 2–4% of the light reflected from the sample was not collected.

REFLECTIVITY ANALYSIS AND FITTING PROCEDURE

The reflectivity \mathcal{R} of the graded medium in which ϵ is a function of both x and ω was calculated by approximating the sample as a stack of dielectric layers each with spatially constant $\epsilon(\omega)$. Thus, for example, the dielectric constant of the j th layer, for the case where only ω_p varies spatially, is given by

$$\epsilon_j = \epsilon(\omega, \omega_p(x_j)), \quad (2)$$

where $\omega_p(x_j)$ is given by Eq. (6), (7), (8), or (9) below, and where the remaining parameters are independent of j . The reflectivity for the structure is computed from the complex reflectivity amplitudes R_j of the j th layer by the iterative expression⁹

$$R_j = e^{2ik_n j \delta} (\rho_{j,j+1} + R_{j+1}) / (1 + \rho_{j,j+1} R_{j+1}), \quad (3)$$

where

$$\rho_{j,j+1} \equiv (n_j - n_{j+1}) / (n_j + n_{j+1}),$$

$$n_j \equiv \sqrt{\epsilon_j}, \text{ and } \delta \equiv x_{j+1} - x_j.$$

The reflectivity \mathcal{R} at the film surface at x_0 is just $|R_0|^2$. This procedure is computationally convenient, but one must be assured that the layers are sufficiently numerous so that their size and number introduces no layer-dependent effects on the computed reflectivity. To ensure this, the number of layers was increased until no significant change in the quality of fit occurred.

The best-fit parameters were obtained by minimizing the value of

$$\chi^2 = (r_i - \mathcal{R}_i)^2 / \Delta r_i^2, \quad (4)$$

where r_i are the ratio spectral data points, \mathcal{R}_i the computed reflectivities (as a function of frequency ω_i and the dielectric parameters), and Δr_i is the standard deviation of the i th point.

MODEL DIELECTRIC FUNCTION-BULK

The theoretical model for the bulk dielectric function has been discussed in some detail by several authors.^{10–13} We note briefly that the low-frequency dielectric properties of PbTe and related compounds have been described with fair success by the two-oscillator dielectric function

$$\epsilon(\omega) = \epsilon_\infty + \frac{\epsilon_\infty(\omega_L^2 - \omega_T^2)}{\omega_T^2 - \omega^2 - i\gamma\omega} - \frac{\omega_p^2}{\omega(\omega + i\nu)}, \quad (5)$$

where ϵ_∞ is the bound charge contribution and is considered a constant, ω_L and ω_T are the longitudinal and transverse optical-phonon frequencies, ω_p is the plasma frequency, and γ and ν are the phonon and plasma linewidths. The longitudinal and transverse modes defined by this function in the usual way correspond closely to the frequencies at which “anomalies” are observed in the reflectivity. These characteristic frequencies are conventionally called ω_- , ω_T^* , and ω_+ in order of increasing frequency. At frequencies above ω_+ , the higher longitudinal-mode frequency of the coupled phonon-plasma system, the medium becomes nearly transparent. The frequency ω_T^* is only slightly shifted from the bare-TO-phonon frequency (for our purposes we shall not distinguish between them) and ω_- corresponds to a low-frequency longitudinal resonance induced in the plasma system by the interaction with the phonons.

MODEL DIELECTRIC FUNCTION-FILM

The basic assumption of our analysis of the epitaxial reflectivity data is that the dielectric model of Eq. (5) may be applied, it being necessary only to allow for spatial dependence of one or more of the parameters. Several of the dielectric param-

eters could be expected to change in going from the surface of the film into the substrate. The analytical approach taken was to perform a χ^2 fit to the data of the reflectivity calculated from Eqs. (3) and (5) using spatially varying dielectric parameters.

The variation of each parameter was modeled as follows:

ϵ_∞ : The values for the high-frequency dielectric constant were chosen from data by Lowney *et al.*¹⁴ Their interference technique is expected to be more accurate and reliable than other methods to determine ϵ_∞ in PbSnTe.

Both the low-temperature reflectivity analysis and a microscopic examination of an etched cross section of the film and substrate indicated a fairly abrupt chemical interface. It was therefore felt that ϵ_∞ , which depended only on the tin concentration at these low-carrier densities, would be adequately modeled by two discrete constant values, one for the film and the other for the substrate. The distance for the change from film to substrate value was taken to be the film thickness obtained from a low-temperature two-layer fit (described below). The exact value of this change over distance was not critical since an error of as much as 2 μm would not appreciably affect the results of our analysis.

ω_L : Like ϵ_∞ , ω_L depends on x and therefore would not be expected to vary significantly within the film. Moreover in the substrate the effects of ω_L on the reflectivity are smaller than those of the plasma. For example, the effect on reflectivity of a 10% difference in ω_L between film and substrate could be offset by a 2% change in the substrate plasma frequency. The data, therefore, are not very sensitive to the value of the substrate ω_L and for simplicity of analysis the value has been taken to be equal to the film value.

γ : The phonon linewidth was assumed to be the same in film and substrate for reasons similar to those given above for ω_L .

ω_T : The spectral reflectivity from 40 to 350 cm^{-1} is rather insensitive to the value of the TO phonon. Therefore, the room-temperature value of 32 cm^{-1} obtained by neutron measurements for¹² PbTe was used for both film and substrate at room temperature. For liquid-N₂ temperatures 20 cm^{-1} was used, this figure having been obtained by interpolation from literature values of PbTe and PbSnTe.^{12,13,15}

ν : Because phonon scattering of the free carriers dominates at room temperature,¹⁶ the film and substrate free-carrier linewidths were assumed to be equal. Hall measurements on platelets of bulk material grown under conditions identical to those for film growth¹⁷ indicate that the film linewidth should decrease 10–20 times on cooling

to liquid-N₂ temperature. The present reflectivity measurements indicate that the substrate linewidth decreases only slightly upon cooling. For low-temperature analysis, it was assumed that the film linewidth was a factor of 10 smaller than the substrate linewidth. Because of the low film plasma density, the data are insensitive to the exact magnitude of the room-temperature and low-temperature film free-carrier linewidths. The approximation is therefore adequate for this analysis.

ω_p : The plasma frequency is equal to $(4\pi Ne^2/m_c)^{1/2}$ where N is carrier concentration and m_c is the conductivity effective mass. Because of its dependence on carrier concentration and effective mass, ω_p is the dielectric parameter with the greatest spatial variation. Four models for the spatial variation of this parameter were tried with varying quality of fit.

Two-layer model: The simplest model used was defined by

$$\omega_p^2 = \begin{cases} \omega_F^2, & 0 \leq x < a \\ \omega_S^2, & a \leq x \end{cases} \quad (6)$$

where x is the distance into the film from the front surface, ω_F is the film plasma frequency, and ω_S is the substrate plasma frequency. This model proved very satisfactory for describing the low-temperature data in the region from 40 to 160 cm^{-1} which extended from the restrahl region through the first minimum and maximum in the reflectivity above ω_* . Because the wavelength of light in the medium in this region is long compared to film thickness, there was no significant difference between the quality of fit obtained for this two-layer model and the quality of fit obtained with the various graded models below. The results of the two layer fit were therefore used to establish values for ω_L and γ at low temperatures. On fitting the entire spectral range, the two-layer model proved much less adequate than any of the graded models.

Exponential model. The functional form of this model was

$$\omega_p^2 = \begin{cases} \frac{\omega_F^2(1 + e^{(x-a)/c})}{1 + e^{-a/c}}, & 0 \leq x \leq x_0 \\ \omega_S^2 [= \omega_p(x_0)], & x_0 < x \end{cases} \quad (7)$$

Tanh model. The functional form of this model was

$$\omega_p^2 = \begin{cases} \alpha + \beta \tanh[(x-a)/c], & 0 \leq x < a \\ \omega_S^2, & a \leq x \end{cases} \quad (8)$$

where $\omega_F^2 = \alpha + \beta \tanh(-a/c)$ and $\omega_S^2 = \alpha$.

Linear-slope model. The functional form of this model was

$$\omega_p^2 = \begin{cases} \omega_F^2, & 0 \leq x \leq a \\ \omega_F^2 + x(\omega_S^2 - \omega_F^2)/c, & a < x \leq a+c \\ \omega_S^2, & a+c \leq x. \end{cases} \quad (9)$$

For these graded models, the layer thickness was chosen so as to select equal arc lengths along the $\omega_p^2(x)$ profile. This is somewhat arbitrary, but it serves the purpose of preventing unduly large ω_p steps at steep regions of the profile.

Because of the difficulties in determining experimentally the absolute magnitude of the reflectivity spectra (discussed in the experimental section), a normalization factor S was included as a fit parameter in our analysis along with the dielectric parameters ω_L , γ , ν , ω_F , ω_S , a , and c .

Because they affect the reflectivity primarily at long wavelengths the values of ω_L , γ , and ω_F were insensitive to surface roughness. However a parameter Δ had to be included to simulate the effect of surface roughness in order to obtain an accurate profile of the carrier concentration. In order to model the effect of surface roughness perfectly, it would be necessary to know the distribution of step heights and widths over the surface. The average distance between steps as determined from a microscopic examination is $\approx 60 \mu\text{m}$. Therefore the experimental wavelengths bracket the average distance. Assuming that the incident wave front is coherent on the order of a wavelength, one might expect that the roughness would average reflected intensities at shorter wavelengths and reflected amplitudes at longer wavelengths. Both averages would tend to reduce the magnitude of interference effects in the reflected spectrum. We have chosen Δ so that the calculated reflectivity \mathcal{R} is actually

$$\mathcal{R} = \left| \frac{\mathcal{R}_0(-\Delta/2) + \mathcal{R}_0^{(0)} + \mathcal{R}_0(\Delta/2)}{3} \right|^2, \quad (10)$$

where the $-\Delta/2$, 0 , and $\Delta/2$ indicate the displacement of the front surface of the film with respect to $x=0$. This amplitude averaging gave a greater reduction in the value of χ^2 than intensity averaging. To average both amplitude and intensity would require the introduction of yet another parameter, a complication which we felt was not warranted by the scope of this study.

In some cases, a change in one fit parameter may be offset by a change in one or more of the other parameters to yield nearly the same value of χ^2 near the minimum. Because of the functional form of ϵ , the two parameters ω_L and ω_F are interdependent in this manner, particularly at low temperatures where γ and ν are small and do not significantly affect the reflectivity.

The result of this interdependence is that the reflectivity spectrum at each temperature ef-

fectively determines the single quantity $(\omega_L^2 + \omega_F^2/\epsilon_\infty)^{1/2}$ rather than the two independent fit parameters, ω_L and ω_F .¹⁸ Because there is no convenient direct way to measure ω_F independently, owing to the presence of the substrate, the reflectivity data by themselves establish only an upper bound for ω_L . To obtain the upper bound value, ω_F is fixed at the smallest value possible at the appropriate temperature and ω_L is fit to the data. For room temperature this value of ω_F is estimated from the intrinsic carrier concentration to be $\approx 200 \text{ cm}^{-1}$. An error of 50 cm^{-1} in our estimate of ω_F would yield a change in the computed ω_L value of only 1 cm^{-1} . At liquid-N₂ temperatures the intrinsic carriers provide a negligible contribution to ω_F . However, the lowest doping density measured for platelets of similar growth conditions is $5 \times 10^{15} \text{ cm}^{-3}$ corresponding to an ω_F of 110 cm^{-1} . As will be shown below in the discussion section, the upper-bound values thus determined probably do not exceed the actual values by more than $1-2 \text{ cm}^{-1}$.

RESULTS

Figure 1 shows the room-temperature spectrum of the film together with the best fits produced by the models for ω_p^2 [Eqs. (6)–(9)]. The reflectivity is highest at the low frequencies because this is the restrahl region. Above ω_+ ($\approx 120 \text{ cm}^{-1}$) the film becomes transparent and reflection from the substrate and film surface interfere to cause Fabry-Perot-like oscillations in the reflected intensity. Minima in the reflected intensity occur when the optical thickness of the film is $I n \lambda / 4$ where n is the refractive index at free-space wavelength λ and I is an odd integer. The first minimum, corresponding to a thickness of $n\lambda/4$, oc-

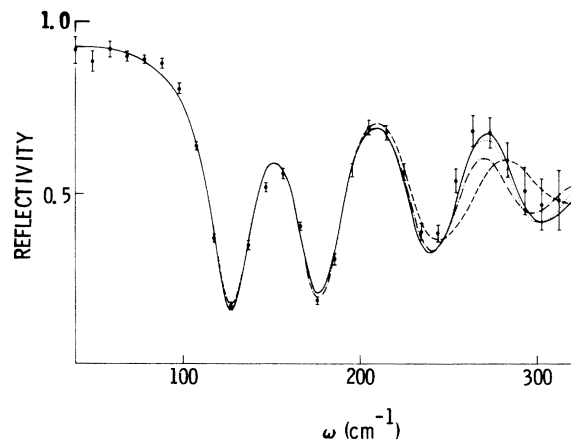


FIG. 1. Room-temperature reflectivity of PbSnTe and accompanying theoretical fits. (—) exponential model; (···) tanh model; (---) linear model; two-layer model.

TABLE I. Dielectric function parameters of PbSnTe epitaxial film at room temperature.

Parameter	Two-layer	Linear	tanh	exp	Estimated statistical errors	Source
$\epsilon_{\infty \text{ film}}$	39	39	39	39		X ray and
$\epsilon_{\infty \text{ sub}}$	44	44	44	44		Ref. 13
ω_L	115.7 cm^{-1}	115.7	115.7	115.7	± 0.3	Present work
ω_T	32 cm^{-1}	32	32	32		See text
γ	17.4 cm^{-1}	18.8	19.0	19.1	± 1.3	Present work
ω_F	245 cm^{-1}	233	205	201	^a	Present work
ω_S	1579 cm^{-1}	1891	1891	1891	± 8	Present work
$\nu_{\text{sub}} (= \nu_{\text{film}})$	99 cm^{-1}	83	81	81	^a	Present work
S	0.99	0.99	0.99	0.99	± 0.01	Present work
Δ	1.28 μm	1.08 μm	1.08 μm	1.12 μm	^a	Present work
χ^2	86	52	42	41		

^a Variations due to modeling are more significant than statistical errors (see text).

curs at 127 cm^{-1} .

Table I summarizes the results of our analysis which was performed as follows:

Step 1. A preliminary fit using the two-layer model was made to the entire curve to establish a value for the film thickness a . For this preliminary fit, Δ , the roughness parameter, was set equal to 0.

Step 2. Fixing a , ν , $\Delta (=0)$, and ω_F (at the room-temperature minimum value of 208 cm^{-1}), the spectral region from 40 to 130 cm^{-1} was fit with a two-layer model varying ω_L , γ , ω_S , and S. The quality of fit, χ^2 , was 7.5 for six independent variables.

Step 3. The values obtained for ω_L and S were then used to fit the full curve with the two-layer ω_p^2 models, varying ω_F , ω_S , a , ν , γ , and Δ .

Step 4. The values obtained for ω_L and S from step 2 were used to fit the graded models, while ω_S was fixed at the value determined directly from a reflectivity measurement of the substrate. (Because the two-layer model gave such a poor fit, ω_S was allowed to vary in that model.) Fit parameters were ω_F , ν , γ , a , c (the grading parameter), and Δ .

Errors listed in Table I for ω_L , γ , and S are statistical estimates based on the fitting at step 2. Error in ω_S is a statistical estimate based on the fit to the substrate reflectivity. Uncertainties in ω_F , ν , and Δ are difficult to determine being somewhat model dependent. Under the assumptions stated above that ω_F is near its minimum value, the errors in ν and ω_F for any given model probably do not exceed the spread of values listed in Table I. The uncertainty in Δ is larger, owing to the simplicity of the roughness model we have chosen (see discussion below).

The ability of this technique to determine the ω_p^2 profile can be seen by considering the difference among the model profiles (shown in Fig. 3) as

compared to the quality of fit. For example, deviations of $\approx 1 \mu\text{m}$ between the linear and exponential models near the substrate cause a change of 15 (or 30%) in χ^2 . The closeness of χ^2 values for the tanh and exponential models is also seen in the near coincidence of their ω_p^2 profiles.

Figure 2 also shows the result of an optical micrographic measurement of the film thickness. This procedure is the only technique other than the one herein described for determining film thickness of epi films on conducting substrates. Moreover, the microscopic measurement determines the position of the *chemical interface* which

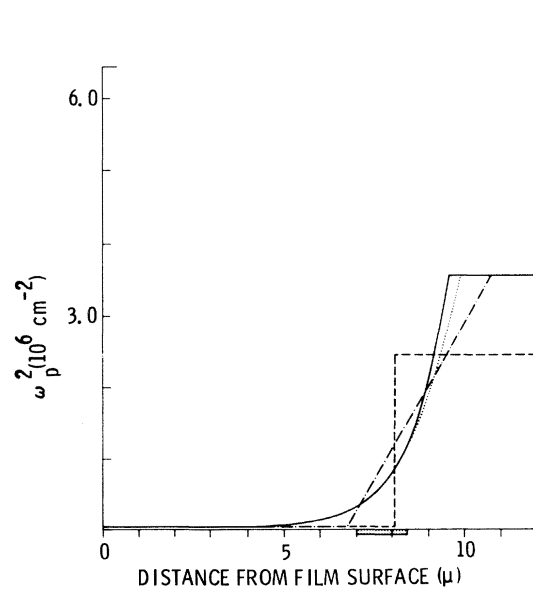


FIG. 2. Room-temperature ω_p^2 profiles. (—)exponential model; (···) tanh model; (---) linear model; (- · -) two-layer model. Dotted area on horizontal axis indicates position of chemical interface as determined by microscopic examination.

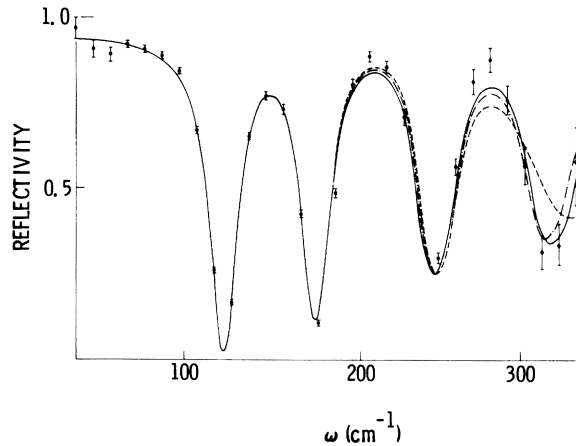


FIG. 3. Liquid- N_2 temperature reflectivity of PbSnTe and accompanying theoretical fits. (—) exponential and tanh models; (- - -) linear model; (· · ·) two-layer model.

is not necessarily in perfect coincidence with the features of the ω_p^2 profile. In the case of our present film, however, the microscopic measurement, although much lower in resolution, shows good agreement with the beginning of the sharp rise in the ω_p^2 profile.

Figure 3 shows the liquid- N_2 temperature spectrum with the best fits to the data given by the various models for ω_p^2 . The data show the same basic features that appear at room temperature. The amplitudes of the interference fringes are larger at low temperatures because of the larger ϵ_∞ and because the phonon and plasma linewidths are smaller. The $n\lambda/4$ minimum has shifted to 123 cm^{-1} . Assuming that ω_L does not change from room temperature to liquid- N_2 temperature, (see discussion section below), the magnitude of this shift closely corresponds to what would be ex-

pected if the film were nearly intrinsic (doping level $\approx 2 \times 10^{16} \text{ cm}^{-3}$).

The fitting procedure was the same for the low-temperature data as for the room-temperature data. However in the low-temperature case for step 2 the frequency range used was $70\text{--}160 \text{ cm}^{-1}$. Lowest frequencies ($40\text{--}60 \text{ cm}^{-1}$) were excluded because the scatter in the data there significantly reduced the fit quality. The higher frequencies ($130\text{--}160 \text{ cm}^{-1}$) were included since the abruptness of the increase in carrier profile at low temperatures more closely resembled the two-layer model and gave a good fit even at frequencies up to 160 cm^{-1} . The χ^2 value for the fit in this region was 4.3 for six degrees of freedom. The main uncertainty in the ω_L bound is the estimate of the carrier concentration in the film (corresponding to $\omega_F = 110 \text{ cm}^{-1}$). Even if the carrier concentration were zero, however, the value of ω_L would increase only $\approx 1 \text{ cm}^{-1}$. The bound thus determined appears to be somewhat lower than could be expected from interpolation of the p - n junction measurements by Nill *et al.*¹⁹

Table II summarizes the results of our low-temperature analysis and Fig. 4 shows the ω_p^2 profiles obtained for the different models. The difference in the value of Δ from room temperature to low temperature is not surprising when one considers that the larger carrier concentration and plasma and phonon linewidths in the film at room temperature act to reduce the amplitude of the interference oscillations in a manner similar to that of surface roughness. Because the linewidth effects are greatest at the longer wavelengths, they apparently obscure the effects of roughness averaging allowing the roughness parameter to better fit the shorter wavelengths where the amplitude-averaging model is less appropriate. This is also consistent with the observation that introducing

TABLE II. Dielectric function parameters of PbSnTe epitaxial film at liquid- N_2 temperatures.

Parameter	Two-layer	Linear	tanh	exp	Estimated statistical errors	Source
$\epsilon_\infty \text{ film}$	46	46	46	46		X ray and
$\epsilon_\infty \text{ sub}$	52	52	52	52		Ref. 13
ω_L	113.5 cm^{-1}	113.5	113.5	113.5	± 0.13	Present work
ω_T	20 cm^{-1}	20	20	20		See text
γ	12.5 cm^{-1}	12.3	11.9	11.7	± 0.5	Present work
$\nu_{\text{sub}} (= \nu_{\text{film}} \times 10)$	43 cm^{-1}	60	73	75	^a	Present work
ω_F	118 cm^{-1}	109	85	71	^a	Present work
ω_S	1170 cm^{-1}	2547	2547	2547	± 30	Present work
S	0.976	0.976	0.976	0.976	± 0.007	Present work
Δ	$0.68 \mu\text{m}$	0.68	0.70	0.70	^a	Present work
χ^2	155	93	76	76		

^aVariations due to modeling are more significant than statistical errors (see text).

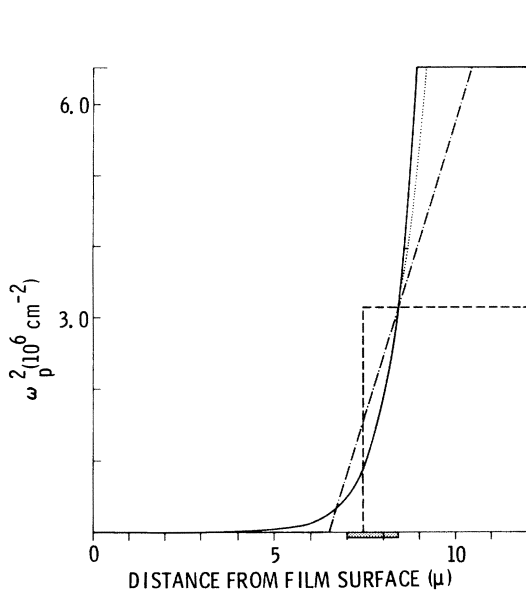


FIG. 4. Liquid-N₂ temperature ω_p^2 profiles. (—) exponential model; (···) tanh model; (-·-·) linear model; (---) two-layer mode. Dotted area on horizontal axis indicates position of chemical interface as determined by microscopic examination.

surface roughness into the model did not reduce the room-temperature χ^2 value as much as the low-temperature value. A more accurate modeling of the surface roughness to include intensity averages as well as amplitude averages would presumably increase the agreement in Δ between the two temperatures.

DISCUSSION

A comparison of the theoretical fits in each temperature range (Figs. 1 and 3) shows that the differences among the models appear most dramatically only at the higher frequencies and are negligible in the region of ω_+ . This fact supports the use of the ω_+ region to establish the phonon parameters as described above.

The fact that the fit quality is significantly better for the graded models than for the two-layer model implies the existence of a few- μ -graded region in the carrier concentration. A further comparison between the continuously graded models (exponential and tanh) and the linear model show that this grading is nonuniform, becoming progressively steep as one might expect because of diffusion of carriers during film growth. The value of χ^2 is sufficiently large to indicate that the statistical quality of fit could be improved with a more flexible model than those used. However, a more extensive model would not improve on the values obtained for ω_L and γ .

The quality of fit for the room-temperature data for this same film in the earlier work⁶ was higher because the data did not cover as large a frequency range and was of poorer quality, having larger error bars on most data points.

In the graded region, where the carrier concentration is no longer nearly intrinsic, ω_p^2 is expected to change on cooling only because of the change in m_c^* . Assuming that m_c^* (room temperature)/ m_c^* (liquid-N₂ temperature) is constant (≈ 1.81)²⁰ throughout the film-substrate interface, one can compare the room-temperature and low-temperature profiles. This comparison is made for the linear and tanh models in Fig. 5. The normalized profiles agree within the accuracy of our technique, the low-temperature profile reaching its value a few tenths of a micron closer to the film surface in both cases. Most of this small discrepancy can be accounted for by the statistical uncertainties in the data and by the uncertainty of a few percent in the values used for ϵ_∞ .

One might expect that the region of gradation in carrier concentration in some way corresponds to the gradation in chemical composition from film to substrate. The sample is *p*-type with the substrate being richer in tellurium and tin. Diffusion of Pb from film into substrate and Te from substrate to film would cause a gradation in the carrier

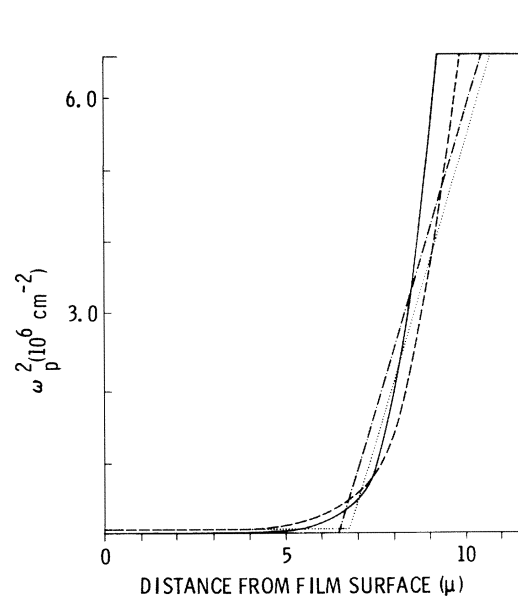


FIG. 5. Normalized ω_p^2 profile of room-temperature (RT) and low-temperature (LT) tanh and linear models. (—) LT tanh; (---) RT tanh; (-·-·) LT linear; (···) RT linear. The profiles have been normalized by the ratio of room-temperature m_c^* to liquid-N₂-temperature m_c^* . The good agreement shown demonstrates the consistency of the present method for determining the carrier concentration profiles.

concentration in the manner indicated. As far as the dielectric properties and reflectivity are concerned, this grading in film properties over $\approx 1-2 \mu\text{m}$ will appear significantly only in ω_p^2 as was indicated above in the discussion of the various parameters. The published values of diffusivity D for self-diffusion of Pb in PbTe would give a diffusion length (D times growth time)^{1/2} of about $0.3 \mu\text{m}$ for the growth conditions of this sample. This length is comparable to, but somewhat smaller than, the $\sim 1\text{-}\mu\text{m}$ diffusion length one might estimate from the figures. The diffusion of Te from the substrate is comparable to that of Pb from the film.

It was mentioned above that the upper-bound figures for ω_L shown in the tables probably do not exceed the actual values by more than $1-2 \text{ cm}^{-1}$. A comparison of the room-temperature neutron results¹² for PbTe with the p - n junction results¹⁹ for PbTe at 4 K indicates that ω_L does not change from 114 cm^{-1} upon cooling. The claimed accuracy of each measurement is $\pm 2 \text{ cm}^{-1}$. This suggests that our film sample, being only 12% Sn, will not

behave in a significantly different manner. The upper-bound values presently obtained for ω_L at the two temperatures agree within the 2-cm^{-1} error both with each other and with the PbTe values. A doping density of only $2 \times 10^{16} \text{ cm}^{-3}$ would reduce ω_L to 111 cm^{-1} at liquid- N_2 temperatures while leaving ω_L at room temperature essentially unchanged at 115 cm^{-1} . This would seem to be too large a change in ω_L in light of the PbTe values.

ACKNOWLEDGMENTS

The authors would like to thank J. E. Clarke for providing the epitaxial film sample and E. R. Gertner for making the x-ray characterizations used to determine Sn content of film and substrate. A. M. Andrews and W. F. Hall made several useful contributions to our understanding of this problem. J. T. Longo provided both helpful advice and data on PbSnTe platelets of film-type material that greatly aided the present analysis. Dr. J. R. Lowney and Professor S. D. Senturia graciously consented to let us use their measurements of ϵ_∞ prior to the publication of their work.

*Work supported by the Office of Naval Research.

¹S. Doniach, Proc. Phys. Soc. London **6**, 849 (1959).

²H. Ehrenreich, J. Phys. Chem. Solids **8**, 130 (1959).

³J. T. Longo, E. R. Gertner, and A. S. Joseph, Appl. Phys. Lett. **19**, 202 (1971).

⁴A. M. Andrews, J. T. Longo, E. R. Gertner, J. G. Pasko, J. E. Clarke, and P. Neuber, in IRIS Detector Speciality Meeting, Washington, D. C., 1973 (unpublished).

⁵A. M. Andrews, J. A. Higgins, J. T. Longo, E. R. Gertner, and J. G. Pasko, Appl. Phys. Lett. **21**, 285 (1972).

⁶W. E. Tennant and J. A. Cape, Appl. Phys. Lett. **26**, 694 (1975).

⁷These values correct the nominal values given in Ref. 6.

⁸H. E. Bennett, M. Silver, and E. J. Ashley, J. Opt. Soc. Am. **53**, 1089 (1963).

⁹This expression results from boundary value matching of electric and magnetic fields at an interface, see for example L. D. Landau and R. M. Lifshitz in *Electrodynamics of Continuous Media* (Pergamon, London, 1960), Chaps. 9 and 10.

¹⁰G. Lucovsky, Richard M. Martin, and E. Burstein, Phys. Rev. B **4**, 1367 (1971).

¹¹E. Burstein, A. Pinczuk, R. F. Wallis in *The Physics of Semimetals and Narrow-Gap Semiconductors*, edited by D. L. Carter and R. T. Bate (Pergamon, New York, 1971), p. 251.

¹²W. Cochran, F. R. S., R. A. Cowley, G. Dolling, and M. M. Elcombe, Proc. Roy. Soc. A **293**, 433 (1966).

¹³M. A. Kinch and D. D. Buss, Solid State Commun. **11**, 319 (1972).

¹⁴J. R. Lowney, S. D. Senturia, and R. L. Aggarwal, Bull. Am. Phys. Soc. **20**, 391 (1975), and private communication with the authors. This technique is es-

entially identical to that applied by Jay N. Zemel, James D. Jensen, and Richard B. Schooler [Phys. Rev. **140**, A330 (1965)] to PbTe. It was first applied by H. R. Riedl and R. B. Schooler, Phys. Rev. **131**, 2082 (1963).

¹⁵G. Dolling and W. J. L. Buyers, J. Nonmetals **1**, 1 (1973).

¹⁶H. A. Lyden, Phys. Rev. **135**, A 514 (1964). Lyden's results for PbTe with carrier concentration comparable to the present substrate carrier concentration indicate the dominance of phonon scattering at room temperature by the T^3 behavior of the mobility. It is possible that for our substrate a significant contribution comes from defects as well in light of the relatively small change in substrate linewidth on cooling. Nevertheless since the low plasma density in the film makes the exact film linewidth relatively unimportant to the quality of fit, our assumption of equal room-temperature linewidths should be adequate.

¹⁷J. T. Longo (private communication).

¹⁸It is easily seen that Eq. (5) in the limit of $\omega \gg \gamma$, ν , ω_T and $\omega_L \gg \omega_T$ reduces to the equation for the film ($\omega_p^2 = \omega_F^2$)

$$\epsilon(\omega) = \epsilon_\infty - (\omega_L^2 + \omega_p^2) / \omega^2$$

The resultant reflectivity varies with the quantity $(\omega_L^2 + \omega_p^2)^{1/2}$ reaching a minimum for ω just above this value.

¹⁹K. W. Nill, J. N. Walpole, A. R. Calawa, and T. C. Harman, in Ref. 11, p. 383.

²⁰The value of ≈ 1.81 for this ratio was obtained by observing the shift in ω_S^2 from room temperature to liquid- N_2 temperature as determined from reflectivity measurements made of the back side (substrate) of the sample. This ratio is supported by the PbTe values of Ref. 16.

²¹M. D. Gomey, D. A. Stevenson, and R. A. Huggins, J. Phys. Chem. Solids **32**, 335 (1971).